PHYSICS OF FLUIDS **24**, 045107 (2012)

Emergence of the four layer dynamical regime in turbulent pipe flow

J. Klewicki,[1,a)] C. Chin,[1] H. M. Blackburn,[2] A. Ooi,[1] and I. Marusic[1]
[1]*Department of Mechanical Engineering, University of Melbourne, Victoria 3010, Australia*
[2]*Department of Mechanical and Aerospace Engineering, Monash University, Victoria 3800, Australia*

(Received 12 July 2011; accepted 13 January 2012; published online 17 April 2012)

Direct numerical simulations of fully developed turbulent pipe flow that span the Reynolds number range $90 \lesssim \delta^+ \lesssim 1000$ are used to investigate the evolution of the mean momentum field in and beyond the transitional regime. It is estimated that the four layer regime for pipe flow is nominally established for $\delta^+ \geq 180$, which is also close to the value found for channel flow. Primary attention is paid to the magnitude ordering and scaling behaviors of the terms in the mean momentum equation. Once the ordering underlying the existence of four distinct balance layers is attained, this ordering is sustained for all subsequent increases in Reynolds number. Comparisons indicate that pipe flow develops toward the four layer regime in a manner similar to that for channel flow, but distinct from that for the boundary layer. Small but discernible differences are observed in the mean momentum field development in pipes and channels. These are tentatively attributed to variations in the manner by which the outer region mean vorticity field develops in these two flows. © *2012 American Institute of Physics*. [http://dx.doi.org/10.1063/1.3702897]

I. INTRODUCTION

The content of this study centers on two primary tasks. One is to document empirically the evolution of the terms in the mean momentum equation for fully developed pipe flow. The other is to interpret the evolution of the terms in the mean momentum equation in the context of a recently developed theory.[3,4]

Evolution of the mean dynamics is studied over a Reynolds number range that begins shortly after the onset of finite velocity fluctuations, and ends with the onset of what is termed the *four layer regime*. The starting Reynolds number is just beyond the upper limit of the laminar regime. With increasing Reynolds number from there, the mean momentum field qualitatively changes owing to an additional (third) non-zero term in the mean momentum equation. Commensurate with this, the magnitudes of the terms in this equation change as a function of radial position. Namely, within three sub-regions the equation is brought into balance owing to two large terms and one small term, while in another sub-region all three terms continue to contribute significantly to the balance. Increasing Reynolds number results in the larger terms in a sub-region to become increasingly larger than the smaller term. Herein we refer to the distinctive relative magnitudes of the terms on any given sub-region (layer) as the *magnitude ordering* of terms affiliated with that layer. The evolution with Reynolds number continues until the magnitude orderings characterizing the four layers are well-established. This defines the onset of the four layer regime.

The theory employed directly leverages the magnitude orderings of the four layer structure to reveal the Reynolds number scaling properties of the mean momentum equation and its solutions, as well as provide physical insights into the operative dynamical mechanisms. One attribute of this

[a)]Also at Department of Mechanical Engineering, University of New Hampshire, Durham, New Hampshire 03824, USA. Electronic addresses: klewicki@unimelb.edu.au and joe.klewicki@unh.edu.

theory is that it employs well-established criteria that distinguishes whether a differential equation will admit a similarity solution. Namely, a normalized form of an equation is a candidate for admitting a self-similar solution if this form remains unchanged as the governing parameters (in this case just the Reynolds number) are varied.[10] These are commonly referred to as *invariant* or *parameter-free* forms. An example of an invariant form from laminar theory is the Blasius equation for boundary layer flow over a flat plate. In this case, the governing equation admits an invariant form over the entire width of the boundary layer. This occurs because all of the terms in the laminar boundary layer equation retain leading order importance across the entire layer.

The situation in turbulent wall-flows is more complex. In this case, the leading order balance changes with wall-normal position, as described above. The theory has revealed, however, that there is a domain near the wall where the balance expressed by the relevant magnitude ordering admits an invariant form under inner normalization (i.e., using the friction velocity and viscosity), and similarly shows that the leading order balance relevant to a domain near the centerline admits an invariant form under outer normalization (i.e., using the pipe radius as the characteristic length).[3,4,8] Thus, the theory provides a cogent basis for the existence and extent of the inner and outer scaling domains. The identification of inner and outer scaling domains is a clear point of agreement with virtually all (semi) theoretical descriptions of turbulent wall-flows, albeit in many treatments these scaling domains are simply assumed to exist.

Where the present theory is most distinct pertains to what happens between the inner and outer domains. In this regard, analysis shows that the governing differential equation formally admits a single invariant form across a continuous hierarchy of scaling layers. Collectively, these scaling layers are termed the L_β hierarchy. In this name the L refers to the layer hierarchy, while the subscript β conveys that the properties of the layer hierarchy, including the distribution of layer widths on the hierarchy, depend upon the parameter β. Perhaps not surprisingly, this parameter is directly related to the mean effect of turbulent inertia (Reynolds stress gradient) that is the new term that appears in the post-instability mean momentum balance. A primary feature of the L_β hierarchy is its inner-normalized layer width distribution, $W(y^+)$. $W(y^+)$ exists on the L_β hierarchy, and, at each wall-normal position on the hierarchy, is the characteristic length that allows the mean momentum equation to be written in its single invariant form. At the lower end of the hierarchy, W is only about four viscous units, and at the upper end it is about a third of the pipe radius. Thus, essentially all of the scales of motion between the inner and outer scaling domains are affiliated with the dynamics on the hierarchy.

With increasing Reynolds number W is increasingly well-represented by a linear function of y^+ on a domain interior to the upper and lower boundaries of the L_β hierarchy. This increasing linearity is inherently tied to the fact that the magnitude orderings associated with the four layer structure become increasingly well-defined as the Reynolds number gets larger. Mathematically, this means that the behaviors on the hierarchy, which are approximately self-similar at any finite Reynolds number, approach exact self-similarity as the Reynolds number increases. This emerging self-similarity physically pertains to the flux of turbulent inertial force across the layers on the hierarchy, and the emergence of a mean velocity profile that is well-approximated by a logarithmic function.

Over the Reynolds number range of the present investigation the properties of the four layer regime just described come into being. In connection with this, recent analyses of low Reynolds number, post-laminar, planar Poiseuille, and zero-pressure-gradient boundary layer flows reveal that the transitional regimes in these flows are also meaningfully characterized in terms of the magnitude ordering of terms in the equation governing their mean dynamics.[1,2] (Note that if a quantity, b, is of leading order magnitude, say $b = O(1)$, then it is taken to mean that both b and $1/b$ remain bounded as the Reynolds number tends to infinity.) The transitional Reynolds number regime is marked by the non-negligible influence of all of the relevant terms in the mean dynamical equation for the channel and boundary layer, respectively. Through the transitional regime, the flow mechanisms associated with the inertia of the turbulent fluctuations cause one of the operative terms to diminish in relative magnitude on each of three of the four emergent layers, whereas in one layer, layer III, all of the terms maintain equal order of magnitude for all Reynolds numbers. In the other three layers, the

observed magnitude disparity increases with increasing Reynolds number, and the scaling properties of the emerging four layer structure become increasingly well-defined.

The beginning of the four layer regime marks the lowest Reynolds number at which one can reasonably assert that the scaling properties derived from the theory of Fife *et al.* are applicable.[3,4] The four layer regime is appropriately described as the asymptotic dynamical regime for turbulent wall-flows, as the magnitude ordering of the terms in the mean momentum balance on each of the layers, and the scaling properties affiliated with these orderings, are increasingly well-established for all higher Reynolds numbers.

Of the three canonical turbulent wall flows (channels, boundary layers, and pipes), the pipe is the only one whose evolution into the four layer regime has not yet been characterized. Thus, the aims of the present study are to document the evolution of the terms in the mean momentum equation that culminates with the onset of the four layer regime in fully developed pipe flow, to estimate the minimum Reynolds number of the pipe flow four layer regime, and to compare and contrast how the four layer regime emerges in the pipe relative to the channel and boundary layer. To set the appropriate context, we first review the primary attributes of the four layer regime.

A. The four layer regime

To within Prandtl's approximations, the laminar regime in the boundary layer is marked by a balance between the time-rate-of-change of streamwise momentum and the retarding viscous force that affects this rate of change. The laminar regime of fully developed flow in channels and pipes is devoid of any time-rate-of-change of momentum, as the mean differential force balance purely comprises a driving pressure force and an equal and opposite viscous force. In the boundary layer the two opposing dynamical effects are equal at every point, but these effects (streamwise advection and viscous force) are varying functions of the distance from the wall, y. For fully developed laminar flow in channels or pipes, the two opposing forces are independent of y.

With the advent of instability, the nonlinear mechanisms affiliated with the inertia of the turbulent fluctuations become increasingly important. The mean effect of these accelerations is accounted for by the gradient of the so-called Reynolds stress in the mean differential force balance. For a pipe of radius δ, the mean momentum balance is given by

$$\frac{\rho}{r}\frac{d(r\langle uv\rangle)}{dr} = -\frac{dP}{dx} + \frac{\mu}{r}\frac{d}{dr}\left(r\frac{dU}{dr}\right), \tag{1}$$

where the (u, v, w) velocity components are associated with the (x, r, θ) coordinate frame. Through the coordinate transformation, $y = \delta - r$, and use of the once-integrated form

$$u_\tau^2\left(1 - \frac{y}{\delta}\right) + \langle uv\rangle = \nu\frac{dU}{dy}, \tag{2}$$

Eq. (1) takes on the same form as for channel flow, i.e.,

$$\frac{d\langle uv\rangle}{dy} = \frac{u_\tau^2}{\delta} + \nu\frac{d^2U}{dy^2}, \tag{3}$$

or in terms of simple notation

$$\mathrm{TI} = \mathrm{PG} + \mathrm{VF}.$$

Here we have employed $\nu = \mu/\rho$ and the boundary condition relating the pressure gradient to the wall shear stress, τ_w, and thus to the friction velocity, $u_\tau = \sqrt{\tau_w/\rho}$. As in the channel, the mean statement of dynamics for the pipe indicates that the net effect of turbulent inertia (TI) is balanced by the sum of the mean pressure gradient (PG) and viscous (VF) forces.

In the transitional regime, all three terms in Eq. (3) are of non-negligible magnitude for all y. With increasing δ^+, the balance expressed by Eq. (3) is, with increasing accuracy, attained owing to two dominant terms in three increasingly distinct layers. Since PG is always independent of y, the emerging (four layer) structure is best illustrated by examining the ratio of VF to TI. A schematic depiction of this ratio is shown in Fig. 1 as a function of y^+ for fixed δ^+ in the four layer regime.

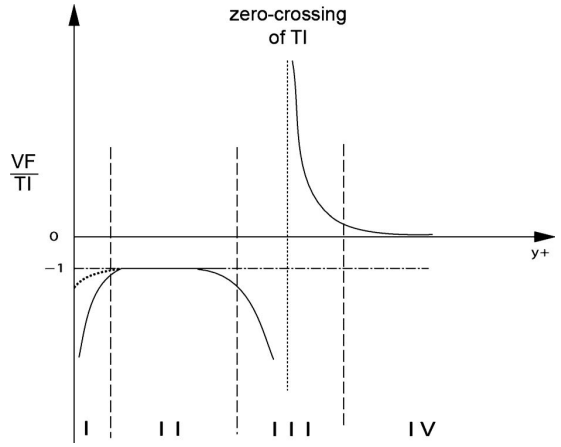

FIG. 1. Sketch of the ratio of the mean viscous force (VF) to mean effect of turbulent inertia (TI). This ratio reveals the four layer force balance structure of turbulent wall-bounded flows.[8] Note that this sketch is for a fixed Reynolds number, as the layer boundaries depend on δ^+. Note also that layer I in the zero pressure gradient turbulent boundary layer (dotted line in I) differs from that of channel or pipe flow. In the boundary layer all of the terms in the mean momentum equation approach zero as $y \to 0$.

Figure 1 effectively depicts the mean free-body diagram for the differential fluid elements at each position $0 \leq y \leq \delta$. Given Eq. (3), a non-trival balance can only occur owing to either two or three co-dominant terms. This balance is attained according to a different magnitude ordering in each of the four layers: layer I, $|\text{PG}| \simeq |\text{VF}| \gg |\text{TI}|$; layer II, $|\text{VF}| \simeq |\text{TI}| \gg |\text{PG}|$; layer III, $|\text{PG}| \simeq |\text{VF}| \simeq |\text{TI}|$; layer IV, $|\text{PG}| \simeq |\text{TI}| \gg |\text{VF}|$. The Reynolds number dependencies associated with the four layer regime are important to understanding the present analyses, and thus these are summarized in Table I. Note that the widths of layers I and IV scale with the traditional inner and outer scales, respectively. Thus, as discussed at the outset and clarified below, the primary distinctions between flow descriptions based upon the four layer structure and more classical descriptions pertain to how the inner and outer domains are connected. The orderings associated with Fig. 1 identify the outer edge of layer III as being where VF loses dominant order in Eq. (3). For all y greater than this position, the mean dynamics are dominated by TI and PG. As indicated by Fig. 1 and the scalings of Table I, this position is located a Δy^+ increment of about $0.6\sqrt{\delta^+}$ beyond the wall-normal position, y_m^+, where $-\langle uv\rangle^+ = T^+$ reaches its maximum value. The position y_m^+ is also the point where TI crosses zero, see Fig. 1. This scaling behavior is true for all δ^+. Quantitatively, the scalings of Table I indicate that layer III is nominally *centered* about y_m^+. This is consistent with the empirical evidence that $y_m^+ \simeq \lambda\sqrt{\delta^+}$, with $\lambda \simeq 1.9$.[9] In contrast to classical notions, the balance of terms reflected by the four layer structure reveals that the inner-normalized width of the sub-domain upon which VF retains dominant order increases like $\sqrt{\delta^+}$ with increasing δ^+. This is a direct consequence of the underlying layer hierarchy.

TABLE I. Scaling behaviors of the layer thicknesses and velocity increments associated with the mean momentum equation in turbulent wall-flows in the four-layer regime, see Fig. 1. Note that the layer IV properties are asymptotically attained as $\delta^+ \to \infty$, see Ref. 5.

Physical layer	Δy increment	ΔU increment
I	$O(\nu/u_\tau)$ $(\simeq 3)$	$O(u_\tau)$ $(\simeq 3)$
II	$O(\sqrt{\nu\delta/u_\tau})$ $(\simeq 1.6)$	$O(U_c)$ $(\simeq 0.5)$
III	$O(\sqrt{\nu\delta/u_\tau})$ $(\simeq 1.0)$	$O(u_\tau)$ $(\simeq 1)$
IV	$O(\delta)$ $(\to 1)$	$O(U_c)$ $(\to 0.5)$

B. The underlying layer hierarchy

As noted above, y_m^+ is the distance from the wall where TI passes through zero. Thus, when interpreted as a force, this term acts like a momentum source for $y^+ < y_m^+$ and a momentum sink for $y^+ > y_m^+$.[5,6] Furthermore, the peak values of TI (inner positive, outer negative) have been shown to bound the continuous L_β hierarchy of scaling layers.[4,7] The primary defining attribute of the L_β hierarchy is that on each of its constituent layers (3) formally admits an invariant form.[3] The inner peak in TI (inflection in T^+ from upward to downward curvature) is located near $y^+ = 7$, and the outer peak in TI (inflection in T^+ from downward to upward curvature) is located near $y/\delta = 0.5$.[2] The properties of the L_β hierarchy are determined by the slope and curvature of $T^+(y^+)$, and with increasing δ^+ self-similar dynamics on the hierarchy are attained as a function of scale. Namely, there is a *balance breaking and exchange* of forces across each layer of the hierarchy that replicates what also occurs across the average layer of the hierarchy, which is layer III of Fig. 1.

An important property of the L_β hierarchy is its layer width distribution, $W(y^+)$. By definition, at any position on the hierarchy W is the inner-normalized length scale that allows Eq. (3) to be written in an invariant form. $W(y^+)$ is therefore accurately described as the *natural* length scale of the mean mechanism of turbulent inertia at any given position on the hierarchy. Within this context, it is significant to note that $W(y^+)$ has been analytically shown to asymptotically scale with distance from the wall,[4,7] and thus constitutes the origin of the *distance from the wall* scaling that is often assumed in turbulent wall-flow analysis.

Moreover, this scaling together with the hierarchy of layers makes it consistent with coherent eddy models based on Townsend's attached eddy hypothesis.[11–13] In these phenomenological models a hierarchy of different size, geometrically similar, eddies is prescribed, with a varying population density per length scale of the eddy. The eddies are "attached" per Townsend's description in that their features scale with their distance from the wall, as do the $W(y^+)$ layers on the L_β hierarchy. Establishing firmer connections between the structure of the L_β hierarchy and the action of the self-similar eddy distributions of the attached eddy hypothesis would seem to naturally provide a theoretical foundation for this phenomenology.

$W(y^+)$ is given by the order of magnitude estimate

$$W(y^+) = O(\beta^{-1/2}), \tag{4}$$

and for pipes and channels the parameter β can be evaluated using

$$\beta = \frac{dT^+}{dy^+} + \frac{1}{\delta^+}, \tag{5}$$

where $T^+ = -\langle uv \rangle^+$. There is a unique (one-to-one) correspondence between the value of β and the y^+ position on the hierarchy. This is made explicit by the definition of the function

$$T_\beta(y^+) = T^+(y^+) + \frac{y^+}{\delta^+} - \beta y^+. \tag{6}$$

This function, which formally defines T^+ in terms of β, is used in the analysis to show that a balance breaking and exchange of forces analogous to that which occurs across layer III for Eq. (1) (see Fig. 1) also occurs as a function of scale (as defined by the W distribution) across each layer of the L_β hierarchy.

Somewhat unexpectedly, analysis of channel flow data reveals that, over an internal domain beginning near the outer edge of layer III, Eq. (4) provides a precise estimate for the value of the leading coefficient in the logarithmic equation for the mean velocity

$$U^+ = \frac{4}{A^2} \ln(y^+ - C) + D. \tag{7}$$

In this equation, C and D are constants of integration. The details of the analysis reveal that C is an offset that effectively shifts the origin to the onset of the hierarchy.[3] Within an internal domain beginning near $y^+ = 2.6\sqrt{\delta^+}$, $W(y^+)$ and A are related by[4,7]

$$A = 2\frac{dW}{dy}. \tag{8}$$

This expression shows that an exactly constant value for A corresponds to an exactly constant slope in the $W(y^+)$ distribution. This equivalent condition is approached as $\delta^+ \to \infty$. The properties of the pipe flow W distribution are explored later using Eq. (4), with β computed using (5).

Relation (8) directly stems from the fundamental definition of A

$$A(\beta) = -\frac{d^2\hat{T}_\beta}{d\hat{y}^2}(\hat{y} = 0). \tag{9}$$

In this expression, T_β is given by Eq. (6), and the *hat* denotes normalization by the corresponding W value on the hierarchy. The position $\hat{y} = 0$ corresponds to where T_β attains its maximum for each respective value of β; the value of β determining both the wall-normal position of the layer, and its $W(y^+)$ width. Thus, within each layer the specific value of T_β attains its maximum value at $\hat{y} = 0$, just as T^+ attains its maximum at y_m^+, which equivalently equals $\hat{y} = 0$ for layer III of Fig. 1. Equation (9) expresses a condition of dynamical self-similarity on the hierarchy. This expression explicitly shows that A = const. results owing to a self-similar flux of turbulent inertial force from one layer to the next on the hierarchy. The present investigation clarifies how this self-similar property emerges as the four layer regime is established through transition pipe flow.

C. Objectives

Key properties reviewed above are used to characterize the onset of the four layer regime in pipe flow. In this regard, it is relevant to note that previous analyses indicate that channel and boundary layer flow develop the four layer structure via distinctly different routes, and that the onset of this regime occurs at different Reynolds numbers: $\delta^+ \simeq 180$ in the channel, and $\delta^+ \simeq 360$ in the boundary layer.[1,2] The reasons for these differences are attributable to the differences in both the governing mean dynamical equation and boundary conditions of these flows. The channel and pipe, however, are both governed by Eq. (3), and thus it is rational to anticipate that the route to the four layer regime will occur similarly in these flows. Owing to their different geometries, however, the boundary conditions of pipe and channel flow are likely to exert different influences on the flow development. These, and other relevant issues, are investigated and elaborated upon further in the data presentation below.

II. NUMERICAL METHODS AND DATA SETS

Direct numerical simulations (DNS) were carried out using a parallel spectral element–Fourier code. The Fourier coordinate requires geometric homogeneity and in this problem that is either in azimuth (leading to a cylindrical coordinate formulation) or along the axis (Cartesian). In either case the remaining planar geometry is discretized using nodal spectral elements with a Gauss–Lobatto–Legendre local mesh in each element, and second-order time integration is employed. For all but the highest Reynolds number data set examined here, the cylindrical coordinate formulation was used; the implementation and convergence properties of this code version were detailed previously,[14] while the Cartesian formulation is similar to earlier works.[15]

Leading simulation parameters are summarized in Table II. At the lower end of the Re_τ range examined, the domain length $L_x = 4\pi\delta$, while at the upper end, $L_x = 8\pi\delta$. It has been shown that for the statistics considered in the present work, the larger length is required for convergence at the upper end of the Re_τ-range, while the shorter length is adequate for $Re_\tau < 500$. [16] Near-wall mesh spacings are within well-established guidelines for wall-based DNS that provide $\Delta y^+ < 1$, $\Delta x^+ < 15$ and $\Delta r\theta^+ < 6$.

For each simulation the collection of statistics was initiated after sufficient time had elapsed to let the flow to reach a statistically steady state, and averaging was conducted for a minimum of 10 wash-through times based on the bulk flow speed and domain length.

TABLE II. Summary of computational parameters.

Re_τ	L_x/δ	Δx^+	$\Delta y^+\|_{\text{wall}}$	$\Delta r\theta^+\|_{\text{wall}}$
91	4π	5.4	0.4	3.6
111	4π	5.8	0.4	3.6
157	4π	8.2	0.6	3.9
171	8π	6.7	0.5	8.4
314	4π	13.2	0.9	6.2
500	8π	6.8	0.1	8.2
1002	8π	7.9	0.6	6.5

III. RESULTS

The onset of the four layer regime is estimated using the criteria previously employed for channel and boundary layer flow.[1,2] This is done by examining the ordering of terms described relative to Fig. 1, as well as the scaling behaviors associated with the layer widths and velocity increments across the layers documented in Table I. Two criteria relating to the ordering of terms in layers II and IV are employed, and then supplemented by verifying the layer scaling properties. In layer II the requisite ordering is given by $|\text{VF}| \simeq |\text{TI}| \gg |\text{PG}|$, while in layer IV it is given by $|\text{TI}| \simeq |\text{PG}| \gg |\text{VF}|$. These orderings are (subjectively) deemed to be satisfied when the smaller of the two dominant terms is at least ten times larger than the smallest term near the middle of the given layer (e.g., when $|\text{TI/PG}| > 10$ in the middle of layer II).

Figure 2 plots the ratio VF/TI in a manner consistent with the depiction of Fig. 1. These profiles indicate that the -1 ratio of layer II emerges from below, and that the -1 ratio is nearly exactly met for the three highest δ^+, and over an expanding y^+ domain with increasing δ^+. The layer II profile evolution in Fig. 2 is very similar to what occurs in the channel, and distinct from the layer II formation in the boundary layer.[2] The trend in the profiles also seems to indicate that in the pipe, layer I becomes thinner with increasing Reynolds number. Although difficult to discern from the figure, the layer IV ratio for the lowest three Reynolds numbers retains nonzero values all the way to the centerline. This persistence of a viscous influence in the outer region of the transitional flow is also similar to what is seen in both the boundary layer and the channel.

Relative to the stated criteria, detailed examination reveals the following. In layer IV TI is smaller than PG (albeit only slightly), and thus according to the criteria the relevant comparison of magnitudes is between TI and VF. For $\delta^+ = 157$, TI attains values more than 22 times that of VF in the inner part of layer IV, but then drops to only about 8 times larger nearer to the centerline. This structure of an interior inertial zone and the re-emergence of outer region viscous influences is also seen, but more subtly, in transitional channel flow DNS, and has been interpreted to be associated

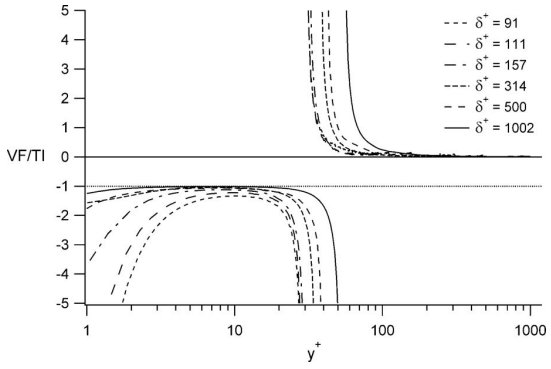

FIG. 2. Ratio of the mean viscous force to the mean effect turbulent inertia in pipe flow for $90 \lesssim \delta^+ \lesssim 1000$.

with the spread of TI toward the periphery.[1] In layer II, however, TI and PG have the same sign and sum to equal VF. Examination of TI relative to PG in layer II at $\delta^+ = 157$ indicates that TI is never more than 8 times larger than PG. Thus, these analyses indicate that the $\delta^+ = 157$ flow is clearly not within the four layer regime. At slightly higher Reynolds number ($\delta^+ = 171$), TI is at least 9.6 times greater than VF throughout layer IV, while TI attains a value of about 9.3 times that of PG in layer II. At this Reynolds number the magnitude ordering criteria are on the verge of being met.

Relative to the layer widths and velocity increments, those associated with layer II have been determined to be most critical. For the $\delta^+ = 171$ flow the measured layer II thickness is 24.4 viscous units, and this varies by about 14% from the value of 21.0 found using approximate scaling formula listed in Table I. Similarly, the layer II velocity increment is about $0.54U_c$ or about 8% different from the value listed in Table I.

Based upon these analyses we conclude that the $\delta^+ = 171$ flow is very close to satisfying the criteria set for the four layer regime. Overall, it is apparent that the δ^+ value marking the onset of the four layer regime in pipe flow is close to that determined for channel flow, i.e., $\delta^+ \simeq 180$. Further evidence supplied below reinforces this assertion, and suggests that the best estimate for the emergence of the four layer structure in pipe flow lies in the range $180 \lesssim \delta^+ \lesssim 200$.

The evolution of the mean dynamics toward the four layer regime is further clarified by examining the profiles underlying the ratios of Fig. 2. These are shown in Fig. 3. Universal features of the VF profile are that it identically equals PG at $y = 0$, is strictly non-positive everywhere, and equals zero at the pipe center. Universal features of the TI profile are that it is zero at the wall, crosses zero at a Reynolds number dependent location, and equals PG at the pipe center. The mechanism of turbulent inertia in wall-flows is spatially localized in an interior zone at the onset of the transitional regime.[1,2] During the early nonlinear development stage of this regime, however, TI spreads both toward the wall and the centerline, until it becomes constrained by the boundary conditions. Relative to the L_β hierarchy, these boundary condition constraints effectively set the minimum and maximum values of $W(y^+)$ such that they attain Reynolds number invariant values that are $O(\nu/u_\tau)$ and $O(\delta)$, respectively. Once this occurs, the inner and outer lengths become parameters relevant to scaling turbulent wall-flows. For turbulent pipe and channel flows, the positions of minimum and maximum $W(y^+)$ identically correspond to the maximal values of $|dT^+/dy^+|$, or equivalently, the inflection points in the T^+ profile. These are denoted by y_{pi} and y_{po}, respectively. As predicted by the theory, these positions increasingly lock into invariant values near $y_{pi}^+ = 7$ and $y_{po}/\delta = 0.5$ as $\delta^+ \to \infty$.

The profiles of y_{pi}^+ and y_{po}/δ versus δ^+ for the present flows are shown in Fig. 4. (Note that for plotting purposes y_{po}/δ is multiplied by 10.) During the transitional regime, both y_{pi}^+ and y_{po}/δ rapidly decrease. Once in the four layer regime, however, they decrease much more slowly. The δ^+ range over which this rate of decrease changes from rapid to slow brackets the noted estimate for the beginning of the four layer regime. The horizontal lines on Fig. 4 denote the estimates of y_{pi}^+ and y_{po}/δ at large δ^+. Thus, it is seen that at $\delta^+ \simeq 180$ y_{pi}^+ is about one viscous unit from its asymptotic

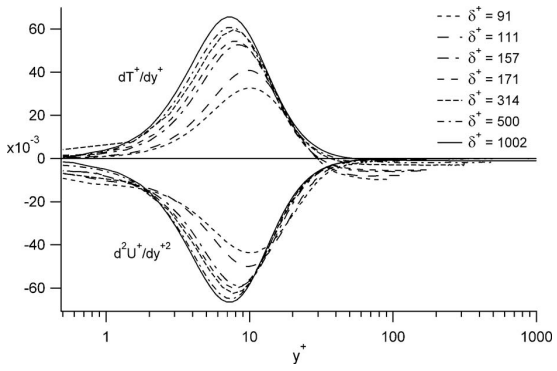

FIG. 3. Inner-normalized mean viscous force and time-averaged turbulent inertia profiles in pipe flow for $90 \lesssim \delta^+ \lesssim 1000$.

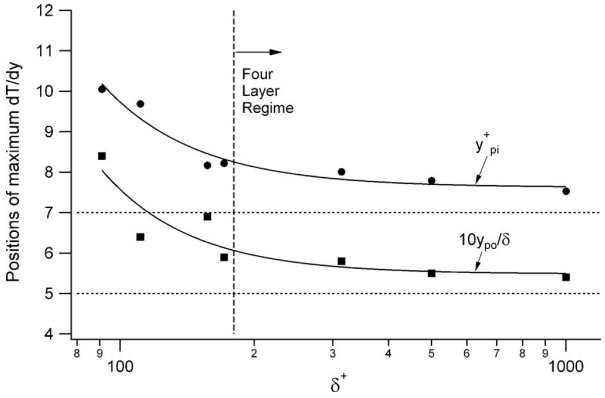

FIG. 4. Positions of the inner and outer maxima of the dT^+/dy^+ profiles of Fig. 3. Note that the inner peak approaches a fixed y^+ value ($y^+_{pi} \simeq 7$), while the outer peak approaches a fixed y/δ value ($y/\delta \simeq 0.5$). The vertical line ($\delta^+ \simeq 180$) indicates the present estimate for the onset of the four layer regime.

value, and by $\delta^+ = 1002$ this difference is approximately halved. Similarly, near the onset of the four layer regime $y_{po}/\delta \simeq 0.6$, and by $\delta^+ = 1002$ $y_{po}/\delta \simeq 0.54$. As with channel flow, both y^+_{pi} and y_{po}/δ approach their high δ^+ values from above. The analogous processes in the boundary layer occur differently.

For the transitional regime boundary layer, y^+_{pi} initially moves very close to the wall and then slowly approaches $y^+ \simeq 7$ from below. There is also some evidence that y_{po}/δ retains values in excess of 0.6 up to considerably larger Reynolds numbers.[2] Note, however, that in the boundary layer y_{po}/δ does not necessarily coincide with the position of W_{max}. This stems from the non-constancy of the mean advection profile.

The significances of y^+_{pi} and y_{po}/δ are further clarified by noting their relationships to the L_β hierarchy and its characteristic length scale distribution, $W(y^+)$. Some of these are depicted in Fig. 5, which shows the profiles of $T^+ = -\langle uv \rangle$ and WdT^+/dy^+ at $\delta^+ = 171$. Since W is the *natural* length scale distribution for the mechanism of turbulent inertia, the weighted profile of dT^+/dy^+ provides a clear graphical depiction of the source and sink character of TI for $y^+ < y^+_m$ and $y^+ < y^+_m$, respectively. At any given δ^+, it is easily shown that the source and sink contributions integrate to zero owing to the boundary conditions on T^+. In Fig. 5 this parity of equal and opposite contributions is exemplified by the approximately equal magnitude positive and negative peak values of WdT^+/dy^+. (Note that with increasing δ^+ the difference between the magnitude of the positive

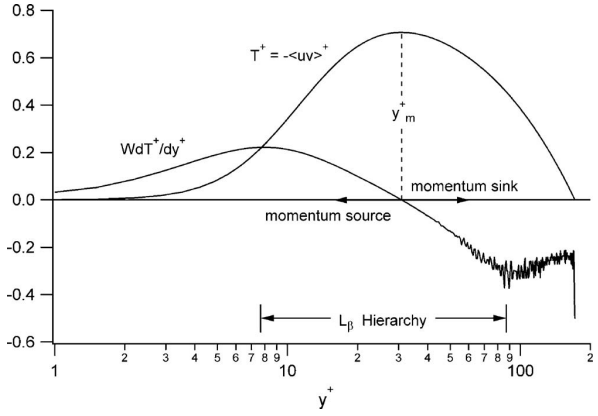

FIG. 5. Profiles of T^+ and WdT^+/dy^+ at $\delta^+ = 171$.

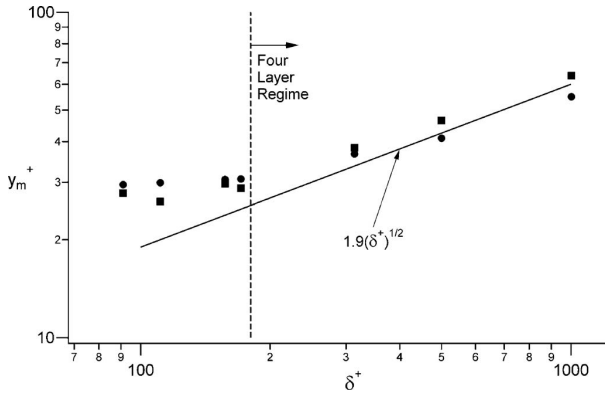

FIG. 6. Actual and predicted values of y_m^+ versus δ^+: actual values, •; values predicted from Eq. (10), ■.

and negative peaks diminishes.) As indicated on the figure, the positions of the peaks also locate the beginning and end of the L_β hierarchy.[2]

Furthermore, since $W(y^+)$ approaches linearity interior to two end points that are moving apart at a rate proportion to δ^+, one can use these end points to estimate the position of the zero-crossing in dT^+/dy^+ (position of maximal T^+, y_m^+). Namely, the theory indicates that

$$y_m^+ = \sqrt{y_{p_i}^+ y_{p_o}^+}, \tag{10}$$

should predict the value of y_m^+ in the four layer regime, and do so with increasing accuracy as $\delta^+ \to \infty$.[2]

Figure 6 compares the actual values of y_m^+ with the prediction of Eq. (10) over the range $90 \lesssim \delta^+ \lesssim 1000$. Prior to the four layer regime, the present data indicate that y_m^+ retains a nearly constant value of about 30. This is different from what is observed in either channel or boundary layer flow, although both exhibit a δ^+ range over which the rate of increase in y_m^+ with increasing δ^+ is less than $\sqrt{\delta^+}$.[1] Within a framework that hypothesizes the existence of an overlap layer, the formulation of Afzal[17] apparently captures this leveling-off effect as a third-order correction to his meso-layer theory. The theory described in Sec. I B is, however, distinct from these and similarly constructed analyses in that it does not rely on the rather prescriptive set of assumptions associated with the overlap layer hypothesis.[4] Instead, it is based upon the properties directly admitted by Eq. (3). This distinction is exemplified by Eq. (10). In contrast, overlap layer based formulations rely on asymptotic expansions of various forms (generally having terms that are cast in powers of Reynolds number), and, owing to the unclosed nature of Eq. (3), have unknown relationship to its solutions.

In the pipe (10) provides a good estimate for the value of y_m^+ even in the transitional regime. This is especially distinct from the behavior of boundary layer flow, where the actual and predicted values only begin to coincide in the four layer regime. Once in the four layer regime, comparison with the reference line indicates that the measured values of y_m^+ increase, but at a rate less than $\sqrt{\delta^+}$. Elsnab *et al.*[1] observed similar behaviors in channel flow. At higher Reynolds numbers, however, both channel and pipe flow data have been shown to be well-fit by $y_m^+ \simeq 2.0\sqrt{\delta^+}$.[8] (In this regard it is relevant to note that the asymptotic estimates for $y_{pi}^+ = 7$ and $y_{po}/\delta = 0.5$ predict that $y_m^+ = \lambda\sqrt{\delta^+}$ with $\lambda = 1.87$.[2]) Consistent with the behaviors depicted in Fig. 4, the data derived from Eq. (10) approach the asymptotic estimate from above, with the last two points adhering to $\lambda = 2.08$ and 2.03, respectively. Overall, the trends of the data in Fig. 6 suggest that the onset of the four layer regime in pipe flow may occur somewhat closer to $\delta^+ = 200$ than 180.

Multiscale analysis that exploits the magnitude ordering of the terms in the four layer regime reveals the conditions under which Eq. (3) will admit a logarithmic mean velocity profile.[3,4] At any finite δ^+, these conditions are only approximately met, but the accuracy of the approximation

improves with increasing δ^+. The theory indicates that logarithmic behavior (approximate or exact) will emerge where the $W(y^+)$ profile first becomes linear (approximately or exactly). As indicated by Eq. (9), an exactly linear W profile physically indicates that the flux of turbulent inertial force is exactly self-similar from one layer to the next on the hierarchy.[7] Analysis of turbulent channel flow reveals that the order of magnitude expression given by Eq. (4) provides an estimate via Eq. (8) for A of 1.25. This corresponds to a value of 0.39 for the von Kármán constant (coefficient) in the traditional logarithmic equation.[7] In the boundary layer, however, while a linear W profile emerges with the advent of the four layer regime, its slope at low δ^+ apparently under-estimates the leading coefficient in Eq. (7) (presuming that C and D have attained constancy in this expression as well). Analysis of available boundary layer data further reveals that, with increasing δ^+, the estimate derived from Eq. (8) improves.[2] The reasons for the differences between the channel and boundary layer were attributed to the fact that the mean advection profile in the boundary layer evolves both in shape and magnitude (while the analogous pressure gradient term in the channel only evolves in magnitude), and the existence of an active vorticity annihilation process in the outer region of the channel (while no such process exists in the boundary layer). This latter process is significant relative to the pipe, since, although there is an active vorticity annihilation process in the outer region, the area over which it must occur diminishes like r as the centerline is approached.

The evolution of the $W(y^+)$ profiles from the present data is shown in Fig. 7. As with the previous analysis of channel flow,[7] the W distribution was found using Eq. (4), with β determined using Eq. (5). As δ^+ increases, a region of increasingly constant slope develops for $y^+ \gtrsim 2.6\sqrt{\delta^+}$, and for y^+ values less than this, the profiles increasingly merge onto a single curve. This latter feature

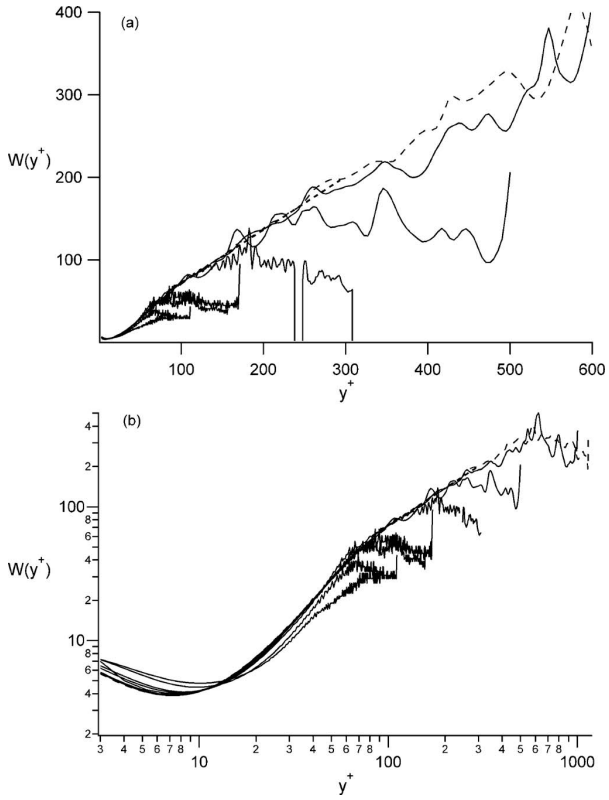

FIG. 7. Layer width distribution of the L_β hierarchy for transitional and four layer regime pipe flow; (a) linear axes and (b) logarithmic axes. Note that the Reynolds number of each profile is given by the end point position $y^+ = \delta^+$ in (b). The curve-fit of the $W(y^+)$ distribution at $\delta^+ = 1002$ is over the range $2.6\sqrt{\delta^+} \leq y^+ \leq \delta^+/3$ and given by $7.52 + 0.644y^+$. The dashed profile is that of Wu and Moin[18] at $\delta^+ = 1142$.

is especially apparent in Fig. 7(b). In accord with the previous estimates for the onset of the four layer regime, these two attributes are first reasonably approximated at $\delta^+ = 171$, and clearly so by $\delta^+ = 314$. The linear profile of Fig. 7(a) demonstrates that the region of approximately constant slope increases in y^+ units. This directly connects to the fact that the upper end of the L_β hierarchy becomes a fixed fraction of δ as δ^+ becomes large, see Fig. 4. Similar to both channel and boundary layer flow, the minimum value of W evolves toward something close to 4 viscous units, while its maximum value evolves to about $\delta/3$. For the purposes of comparison with the previous analysis of channel flow, the $\delta^+ = 1002$ W profile was fit by a linear curve over the domain $2.6\sqrt{\delta^+} \lesssim y^+ \lesssim \delta/3$. This yields a slope of $A/2 = 0.644$, which corresponds to a von Kármán coefficient of about 0.415. For comparison, a curve-fit of the W profile from the $\delta^+ = 1142$ pipe flow DNS of Wu and Moin[18] yields a nearly identical result. Although the data uncertainties preclude any firm conclusions at this time, the slightly higher value than found in the channel is observationally consistent with previous estimates for the logarithmic profile slope found using direct curve-fits of the mean profile itself,[19,20] and physically with the less efficient mechanism of vorticity annihilation in the pipe relative to the channel mentioned above. These physics are further supported by the similar, but more clearly evident phenomena observed in the boundary layer (which has no imposed vorticity annihilation process in the outer region), and the observations made relative to Fig. 2 indicating that the appearance of outer region viscous effects are more apparent in transitional pipe DNS than in channel DNS at the same δ^+.

IV. DISCUSSION AND CONCLUSIONS

The mean dynamical equation for pipe flow can be cast into a form that is identical to that for channel flow. It is thus not surprising that the transitional flow evolution toward the four layer regime in these two flows is similar, and different from what occurs in the boundary layer. Characteristic traits shared by these two flows include the approach from above of y_{pi}^+ and y_{po}/δ toward their high δ^+ values (Fig. 4), and the approach of the y_m^+ prediction of Eq. (10) to the high δ^+ trend from above (Fig. 6).

From the present analysis we conclude that the onset of the four layer regime occurs at nominally the same Reynolds number ($\delta^+ \simeq 180$) as it does in the channel, although some of the data features seem to suggest that it may occur at a slightly higher value than in the channel, say $\delta^+ \simeq 200$. In either case, however, this starting δ^+ value is distinctly different from the $\delta^+ \simeq 360$ value found for the boundary layer. Furthermore, examination of the existing literature indicates that the estimated beginning of the four layer regime in pipe flow occurs well after the initial rapid rise in the skin friction coefficient associated with the establishment of self-sustaining turbulent fluctuations. This is also very similar to what happens in the channel, and different from the boundary layer, where existing evidence indicates that the onset of the four layer regime nominally coincides with the δ^+ at which the skin friction coefficient attains its maximum value.[2]

While exhibiting close similarities with channel flow, the present data also suggest some more subtle differences. One of these is that y_m^+ exhibits effectively constant values over a range of δ^+ during the transitional regime, while in channel flow y_m^+ continuously increases. A second is the evidence that the slope of the $W(y^+)$ profile is slightly larger than found in the channel. This latter observation is made more explicit by the comparison of Fig. 8, which shows pipe and channel flow W profiles at $\delta^+ \simeq 1000$. As indicated, the linear curve-fit of the W profile from the channel DNS at $\delta^+ = 1016$ has a slope of about 0.623. According to Eq. (8), this corresponds to a von Kármán coefficient of about 0.388, which is in very good agreement with the previous estimate found for channel flow of 0.39.[7,22,23] At present, our best hypothesis is that these differences, and indeed many of the differences between boundary layers, pipes, and channels are attributable to the mechanisms influencing the establishment of the outer region mean vorticity profile. Among the three flows, the channel is arguably most effective at accommodating an outward flux of vorticity. The boundary condition on this flow imposes a vorticity annihilation process that acts over a constant planar area as $y/\delta \to 1$. On the other hand, while there is the same boundary condition in the pipe, the cylindrical areas over which this inherently diffusive process must occur is getting smaller like the difference, $\delta - y$, as $y/\delta \to 1$. In contrast, the mean vorticity distribution in the boundary layer is governed by

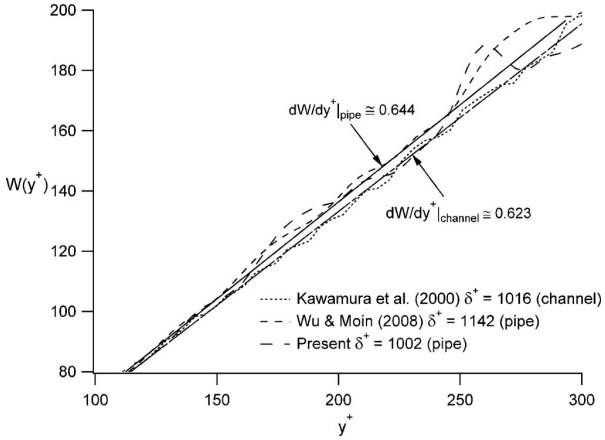

FIG. 8. Comparison of the linear portion of the $W(y^+)$ profiles from channel and pipe flow at $\delta^+ \simeq 1000$. Data are from the present simulation, $\delta^+ = 1002$, the pipe flow simulation of Wu and Moin,[18] $\delta^+ = 1142$, and the channel flow simulation of Kawamura *et al.*,[21] $\delta^+ = 1016$.

the outward advection of vorticity, as modified by the entrainment of irrotational freestream fluid, but without any vorticity annihilation explicitly imposed by the boundary conditions.

ACKNOWLEDGMENTS

The authors gratefully acknowledge the financial support of the Australian Research Council and the computational resources of the Australian Partnership for Advanced Computing (MAS Grant Nos. p46, m45, and d77), as well as the Victorian Partnership for Advanced Computing (Project Nos. pMelb0037 and pMelb0061). Thanks are also extended to Dr. X. Wu and Dr. P. Moin, and Dr. H. Kawamura, Dr. H. Abe, and Dr. K. Shingai for making their simulation data bases available on the internet.

[1] J. Elsnab, J. Klewicki, D. Maynes, and T. Ameel, "Mean dynamics of transitional channel flow," J. Fluid Mech. **678**, 451 (2011).
[2] J. Klewicki, R. Ebner, and X. Wu, "Mean dynamics of transitional boundary layer flow," J. Fluid Mech. **682**, 617 (2011).
[3] P. Fife, J. Klewicki, P. McMurtry, and T. Wei, "Multiscaling in the presence of indeterminacy: Wall-induced turbulence," Multiscale Model. Simul. **4**, 936 (2005).
[4] P. Fife, J. Klewicki, and T. Wei, "Time averaging in turbulence settings may reveal an infinite hierarchy of length scales," J. Discr. Contin. Dyn. Syst. **24**, 781 (2009).
[5] J. Klewicki, P. Fife, T. Wei, and P. McMurtry, "A physical model of the turbulent boundary layer consonant with mean momentum balance structure," Philos. Trans. R. Soc. London, Ser. A **365**, 823 (2007).
[6] G. Eyink, "Turbulent flow in pipes and channels as cross-stream 'inverse cascades' of vorticity," Phys. Fluids **20**, 125101 (2008).
[7] J. Klewicki, P. Fife, and T. Wei, "On the logarithmic mean profile," J. Fluid Mech. **638**, 73 (2009).
[8] T. Wei, P. Fife, J. Klewicki, and P. McMurtry, "Properties of the mean momentum balance in turbulent boundary layer, pipe and channel flows," J. Fluid Mech. **522**, 303 (2005).
[9] K. Sreenivasan and A. Sahay, "The persistence of viscous effects in the overlap region and the mean velocity in turbulent pipe and channel flows," in *Self-Sustaining Mechanisms of Wall Turbulence*, edited by R. Panton (Computational Mechanics Publication, Southampton, 1997), p. 253.
[10] A. G. Hansen, *Similarity Analysis of Boundary Value Problems in Engineering* (Prentice-Hall, 1964).
[11] A. A. Townsend, *The Structure of Turbulent Shear Flow* (Cambridge University Press, 1976), Vol. 2.
[12] A. E. Perry, S. M. Henbest, and M. S. Chong, "A theoretical and experimental study of wall turbulence," J. Fluid Mech. **165**, 163 (1986).
[13] A. E. Perry and I. Marusic, "A wall-wake model for the turbulence structure of boundary layers. Part 1. Extension of the attached eddy hypothesis," J. Fluid Mech. **298**, 361 (1995).
[14] H. M. Blackburn and S. J. Sherwin, "Formulation of a Galerkin spectral element–Fourier method for three-dimensional incompressible flows in cylindrical geometries," J. Comput. Phys. **197**, 759 (2004).
[15] D. Chu, R. D. Henderson, and G. E. Karniadakis, "Parallel spectral element–Fourier simulation of turbulent flow over riblet-mounted surfaces," Theor. Comput. Fluid Dyn. **3**, 219 (1992).

[16] C. Chin, A. Ooi, I. Marusic, and H. M. Blackburn, "The influence of pipe length on turbulence statistics computed from DNS data," Phys. Fluids **22**, 115107 (2010).
[17] N. Afzal, "Analysis of instantaneous velocity vector and temperature profiles in transitional rough channel flow," J. Heat Transfer **131**, 064503 (2009).
[18] X. Wu and P. Moin, "A direct numerical simulation study on the on the mean velocity characteristics in turbulent pipe flow," J. Fluid Mech. **608**, 81 (2008).
[19] H. Nagib and K. Chauhan, "Variation of von Karman coefficient in canonical flows," Phys. Fluids **20**, 101518 (2008).
[20] I. Marusic, B. J. McKeon, P. A. Monkewitz, H. M. Nagib, A. J. Smits, and K. R. Sreenivasan, "Wall-bounded turbulent flows: Recent advances and key issues," Phys. Fluids **22**, 065103 (2010).
[21] H. Kawamura, H. Abe, and K. Shingai, "DNS of turbulence and heat transport in a channel flow with different Reynolds and Prandtl numbers and boundary conditions," in *Proceedings of the 3rd Int. Symp. Turbulence, Heat and Mass Transfer* (Aichi Shuppan, Japan, 2000), p. 15.
[22] J. P. Monty, N. Hutchins, H. C. H. Ng, I. Marusic, and M. S. Chong, "A comparison of turbulent pipe, channel and boundary layer flows," J. Fluid Mech. **632**, 431 (2009).
[23] J. P. Monty and M. S. Chong, "Turbulent channel flow: comparison of streamwise velocity data from experiments and direct numerical simulation," J. Fluid Mech. **633**, 461 (2009).